Molecular Crystals and Liquid Crystals
Publication details, including instructions for authors and subscription information:
http://www.tandfonline.com/loi/gmcl16

# Two Photon Excitation Spectra of the Phenanthrene Crystal

V. Sethurman [a], M. C. Edelson [a], C. K. Johnson [a], C. Sethurman [a] & G. J. Small [a]

[a] Ames Laboratory-USDOE and Department of Chemistry, Iowa State University, Ames, Iowa, 50011, U.S.A.

Version of record first published: 14 Oct 2011.

To cite this article: V. Sethurman , M. C. Edelson , C. K. Johnson , C. Sethurman & G. J. Small (1980): Two Photon Excitation Spectra of the Phenanthrene Crystal, Molecular Crystals and Liquid Crystals, 57:1, 89-117

To link to this article: http://dx.doi.org/10.1080/00268948008069820

*Mol. Cryst. Liq. Cryst.*, 1980, Vol. 57, pp. 89–118
0026-8941/80/5701-0089$04.50/0

Printed in U.S.A.



# Two Photon Excitation Spectra of the Phenanthrene Crystal

## Manifestations of the exciton–phonon and intramolecular vibronic coupling†

V. SETHURAMAN,‡ M. C. EDELSON, C. K. JOHNSON, C. SETHURAMAN and G. J. SMALL

*Ames Laboratory-USDOE and Department of Chemistry, Iowa State University, Ames, Iowa 50011, U.S.A.*

Polarized two-photon excitation spectra associated with the lowest absorption system of the phenanthrene crystal at $T \sim 4.2$ K are reported. Intensity analyses for different principal faces reveal that the dominant intermediate states for the two-photon mechanism derive from molecular states of $B_2(L)$ symmetry. This finding is consistent with theoretical calculations. The spectra principally associated with intermediate states of $A_1(M)$ symmetry exhibit dramatic manifestations of intramolecular vibronic coupling which are in qualitative accord with coupling calculations. The origin region associated with the lower and upper Davydov components exhibits a marked dependence on photon propagation direction **k** and polarization. Included here are the center of gravity and profile of the so-called upper Davydov component. These results are discussed in terms of the exciton-phonon interactions.

## I. INTRODUCTION

Two-photon absorption spectroscopy of organic solids is a valuable methodology for probing electronic and vibrational structure at the molecular level and, just as importantly, the collective excitations and their various interactions associated with the solid. Included here are polariton effects,[1,2] the exciton-phonon interaction, two-particle transitions[3] and the band structure for Frenkel excitons.[3,4] Given the special nature of this journal issue it is particularly appropriate to be reminded of Vladimir Broude's pioneering contributions in the latter two areas.[5,6]

† Work performed in part for the Division of Basic Energy Sciences of the Department of Energy under Contract No. W-1405-eng-82.

‡ Current address: James Franck Inst., 5640 Ellis Ave., Univ. of Chicago, Chicago, IL 60637, U.S.A.

In this paper we examine the polarized two-photon excitation (TPE) spectra of the phenanthrene crystal associated with the lowest energy 350 nm $^1A_1$ state of the free molecule. This state is both one- and two-photon allowed so that a comparison of the one-photon[7–9] and TPE spectra presents interesting possibilities for understanding the intramolecular vibronic coupling via $a_1$ fundamentals which characterizes[7,8,10] the 350 nm state. In addition to this, our interest is in examining the potential of TPE spectroscopy for studying the exciton band structure and exciton-phonon interaction associated with the aforementioned transition. These diverse topics are considered here along with the possible complications of two-photon resonantly driven second harmonic generation (SHG)[11] on the TPE experiment.

## II. ORIENTED GAS POLARIZATION RATIOS FOR PHENANTHRENE

The oriented gas model provides a useful starting point for extracting information on the TPA mechanism at the molecular level from relative TPA cross-sections for the crystal. Monoclinic crystals of phenanthrene belong to the space group $P_{2_1}$ with two molecules per unit cell.[12] A twofold screw axis parallel to the crystal **b** axis relates the two molecules in the unit cell. The phenanthrene molecule possesses $C_{2v}$ point symmetry with the Mulliken axis convention correlating the long (L), median (M) and normal (N) axes with the $A_1$, $B_2$ and $B_1$ reps, respectively. The L axis is nearly parallel to the obtuse bisectrix axis **c*** and the M axis makes an angle of $\sim 28^\circ$ with the **b** axis. The direction cosines are given in Table I with those for the second molecule differing by a change of sign everywhere except the *b* column.

TABLE I

Direction cosines for the phenanthrene crystal

| | *a* | *a** | *b* | *c** | *c*′ |
|---|---|---|---|---|---|
| L | 0.255 | 0.071 | −0.086 | 0.993 | 0.963 |
| M | 0.441 | 0.469 | −0.876 | −0.109 | −0.195 |
| N | −0.861 | −0.880 | −0.474 | 0.020 | 0.185 |

The unit cell group is isomorphic with the point group $C_2$. It is only for the reduced wavevector $\mathbf{k} = 0$ or parallel to the screw axis **b** that the unit cell exciton wavefunctions can be classified according to the *A* and *B* reps of $C_2$. In the static lattice approximation the selection rule $\mathbf{K} = \mathbf{k} \approx 0$, where **K** is the photon wavevector, for transitions between the ground and intermediate states and between the latter and the final states can be utilized. In this section we assume the static lattice approximation. Thus, the crystal states coupled

TABLE II

Molecular transition moment projections

| Initial (final) state, 1 | Final (initial) state, 2 | Transition moment ($\times D_{12}$) $\varepsilon \parallel \mathbf{a}^*$ | $\varepsilon \parallel \mathbf{b}$ | $\varepsilon \parallel \mathbf{c}^*$ |
|---|---|---|---|---|
| $A_1$ | $A_1$ | 0.469 | −0.876 | −0.109 |
| | $B_1$ | −0.880 | −0.474 | 0.020 |
| | $B_2$ | 0.071 | −0.086 | 0.993 |

by the radiation field correspond to the symmetric $|+\rangle$ ($A$) and antisymmetric $|-\rangle$ ($B$) linear combinations of the localized site exciton wavefunctions of the unit cell. For the case in hand where the two-photon transition at the molecular level is to a final electronic state of $A_1$ symmetry we need only consult Table II for polarization analysis of the TPA spectra. For example, since the $B$ rep is antisymmetric with respect to screw axis rotation, it is clear that for the transverse photon polarization parallel and perpendicular to the **b**-axis, the nonvanishing one-photon factor group transitions are $|\pm\rangle \rightarrow |\pm\rangle$ and $|\pm\rangle \rightarrow |\mp\rangle$ respectively. Thus, for a molecular transition $A_1 \leftarrow A_1$,

$$\left|\frac{\langle A_1 \pm |\mathbf{b}\cdot\mathbf{d}|A_1 \pm\rangle}{\langle A_1 \mp |\mathbf{a}^*\cdot\mathbf{d}|A_1 \pm\rangle}\right| = \frac{0.876}{0.469},$$

while for a $B_2 \leftarrow A_1$ transition,

$$\left|\frac{\langle B_2 \mp |\mathbf{c}^*\cdot\mathbf{d}|A_1 \pm\rangle}{\langle B_2 \mp |\mathbf{a}^*\cdot\mathbf{d}|A_1 \pm\rangle}\right| = \frac{0.993}{0.071}.$$

In these expressions **b**, **c*** and **a*** are unit polarization vectors while **d** is the dipole moment operator. With the section rules above it follows immediately, since the ground state is $|A_1 +\rangle$, that only two-photon transitions to $|+\rangle$ factor group states are allowed for both photons polarized either parallel or perpendicular to the **b** axis. This is not the case for cross-polarization experiments. Intensity considerations for this situation are aided with the notationally simplified TPA matrix element

$$M_{fg} = \sum_n \frac{\langle f|\varepsilon\cdot\mathbf{d}|n\rangle\langle n|\varepsilon\cdot\mathbf{d}|g\rangle}{\hbar\omega - E_n} \tag{1}$$

$$\equiv \sum_{i,j} C_i C_j T_{ij}, \tag{2}$$

for the $f \leftarrow g$ transition and unit incident polarization vector

$$\varepsilon = \sum_i C_i \varepsilon_i, \qquad i = \mathbf{a}^*, \mathbf{b}, \mathbf{c}^*. \tag{3}$$

When the transverse photons are perpendicular to the **b** axis with, say, polarization at an angle $\theta$ with respect to one of the other indicatrix axes, say **a***, Eqs. (1) and (3) show that the $|-\rangle$ factor group state is accessible via absorption of one photon polarized along **b** and the other along **c***. Of course the $|+\rangle$ factor group state is also allowed. The details of calculating the intensity ratio $I_+/I_-$ for birefringent crystals are given by Hochstrasser and Sung.[13]

## III. EXPERIMENTAL

### Sample preparation

The phenanthrene used in this study was either fluorescence-grade phenanthrene (Eastman Kodak) purified by zone-refining (60 passes), or 98% phenanthrene (Aldrich Chemical) purified by treatment with maleic anhydride to remove anthracene, by sodium fusion to remove fluorene and other impurities, followed by vacuum sublimation, column chromatography, vacuum sublimation again, and zone-refining (80 passes). The spectra of the Eastman zone-refined material were essentially identical to the spectra of the more extensively purified material.

Crystals grown in a conventional Bridgeman furnace were oriented conoscopically using a polarizing microscope. The *ab* face of phenanthrene was cleaved from a crystal boule, and then crystal sections normal to the optical indicatrices of phenanthrene were prepared. The experimentally determined angle between the *a* axis and the acute bisectric ($a^*$) was *ca.* 16°, differing from the 11° value cited by Winchell.[15] Crystals were polished with an ethanol-soaked tissue prior to mounting in a Janis Super Varitemp 8DT helium cryostat. Spectra were normally obtained with the liquid helium level held just below the crystal. In this way the sample temperature was maintained constant at *ca.* 6 K.

### Spectrometers and detection

The spectra of the origin region were generated using a nitrogen-laser-pumped dye laser (National Research Group PTL-2000). This dye laser incorporates an oscillator-amplifier arrangement and, when used with an intracavity etalon, is capable of *ca.* $6 \times 10^{-4}$ nm resolution. The features of the two-photon spectrum of phenanthrene are quite broad, even at low temperatures, and it was possible to dispense with the etalon for these experiments. The laser was used with a $8 \times 10^{-4}$ M nile blue/$3.8 \times 10^{-3}$ M rhodamine 610 dye solution (Exciton Chemical) in ethanol and had a measured power of 10–20 kW/pulse at 15 Hz, with a linewidth of *ca.* $3–7 \times 10^{-2}$ nm.

A Glan–Thompson prism was installed after the oscillator in order to polarize the input to the amplifier section of the dye laser. The electric vector of the output beam was polarized (polarization ratio > 75:1) and could be rotated to a new orientation by a double Fresnel rhomb. A 50 cm focal length lens focused the beam onto the crystals.

A small fraction of the dye laser output beam was reflected at near-normal incidence by a beam splitter to a spectrally flat laser monitor phototube (RCA 4832). Fluorescence generated via two-photon absorption was detected at right angle to the incident photon propagation direction with a high gain photomultiplier (Amperex 56AVP) shielded from scattered laser light by a 7–37 Corning glass filter and a 7–54 Corning filter specially coated to reduce its deep red transmission. Photomultiplier currents were detected by a two-channel laser photometer (Lambda Physik LF300) which averaged ten signal and reference pulses and then divided the fluorescence signal by the reference laser signal. The peak intensities were eventually normalized to the square of the laser intensity by correcting for the gain curve of the dye laser. Wavelengths were measured by calibrating the dye laser grating drive against a 1.5 m Jobin–Yvon spectrometer.

The two-photon spectrometer used to obtain the spectrum above the origin region has been described in detail elsewhere.[16] The 630–690 nm region covered with a Chromatix CMX-4 flashlamp-pumped dye laser with a laser linewidth of 0.15 nm using rhodamine 640 dye (Exciton Chem.). The laser beam was linearly polarized by a Glan-Thompson polarizer and its electric vector rotated by a double Fresnel rhomb. The beam was focused onto the crystal by a 10 cm focal length lens. The fluorescence resulting from two-photon excitation was collected at right angle to the incident photon direction and condensed by a 5 cm focal length lens onto an Amperex AVP photomultiplier tube shielded from scattered laser light by a combination of Corning CS7-60 and CS7-51 filters. The shape and strength of the laser pulse was monitored by a RCA 4832 photomultiplier. Neutral density filters were used to keep output voltages of laser and fluorescence detectors in the range 0.1 to 0.4 V across a 50 Ω impedance. These outputs were amplified by a Lecroy 10× amplifier (rise time *ca.* 1 ns) before processing.

The laser and reference signals obtained with the flashlamp-pumped dye laser were sampled at several time intervals subsequent to the origin of the laser pulse and digitized to 8 bit accuracy as described by SethuRaman *et al.*,[16] and then reconstructed by linear interpolations on a PDP-8 mini computer (Digital Equipment Corp.). Since the duration of the laser pulse was comparable to the fluorescence lifetime it was necessary to deconvolute the shape of the laser pulse from the decay of the two-photon excited state. Cross sections were determined by trying a series of values of the total decay constant of the excited state and examining the trend of the resulting

cross section for each laser pulse, since each sampling interval of a laser pulse yields a two-photon cross section. It was found empirically that the set of cross sections obtained for each pulse were close to each other for only a very narrow range of decay constants $\gamma$. This narrow range of $\gamma^{-1}$ was found to be independent of two-photon frequency and equal to $50 \pm 20$ ns. Using this $\gamma$, two-photon cross sections were obtained at each frequency by determining a statistically refined average of a set of five laser pulses.

## IV. RESULTS

In what follows the polarized TPE spectra are labelled according to the convention $\mathbf{K}(\mathbf{e}_1, \mathbf{e}_2)$ where **K** defines the propagation direction of the incident transverse photons perpendicular to the crystal face containing the vectors $\mathbf{e}_1$ and $\mathbf{e}_2$. These two vectors define the polarization for the two photons "1" and "2". For spectra where $\mathbf{e}_1 \perp \mathbf{e}_2$ and $\mathbf{K} \perp \mathbf{b}$ the incident photon polarization bisects the $\pi/2$ angle between the two principal axes of the "visible" indicatrix contained in the face perpendicular to **K**. These spectra are a summation of a crossed polarization and two diagonal polarization spectra, cf. section II. The TPE vibronic frequencies reported here are vacuum corrected and vibrational frequencies are measured relative to 29627 $cm^{-1}$ which, according to Craig and Gordon,[7] is the midpoint between the zero-point lower and upper Davydov components located at 29597 and 29657 $cm^{-1}$. Polarization of these two components in the one-photon absorption spectrum[7] is perpendicular to **b** ($\perp$ **b**) and parallel to **b**, respectively. The origin transitions associated with the Davydov components will be referred to as $O_L$ and $O_U$.

Figures 1–4 represent the **b(c*c*)**, **b(a*a*)**, **c′(bb)** and **c′(aa)** spectra obtained at $T \sim 6$ K with the FLPDL and associated detection system (cf. section II). Only the frequency region including the 394 $cm^{-1}$ intramolecular fundamental and to higher energy of it is shown. Reproducibility of these spectra as judged by repeated scans of the same crystal or spectra obtained with different crystals is good. Again the normalization procedure employed bypasses problems associated with laser pulse shape jitter. More recent data obtained with the NPDL system (cf. section II) for selected regions show no significant reduction of the linewidths in Figures 1–4 (typically 10–20 $cm^{-1}$). In addition, the vibrational intensity distributions of the **c′(bb)** and **c′(aa)** spectra are not significantly different from those for the **c*(bb)** and **c*(a*a*)** [also, **c′(a*a*)**] spectra, respectively.

In this paper attention is confined to the origin region and the principal intramolecular fundamental vibrations (primarily those possessing $a_1$ symmetry) and their overtones and combinations. Weaker features associated

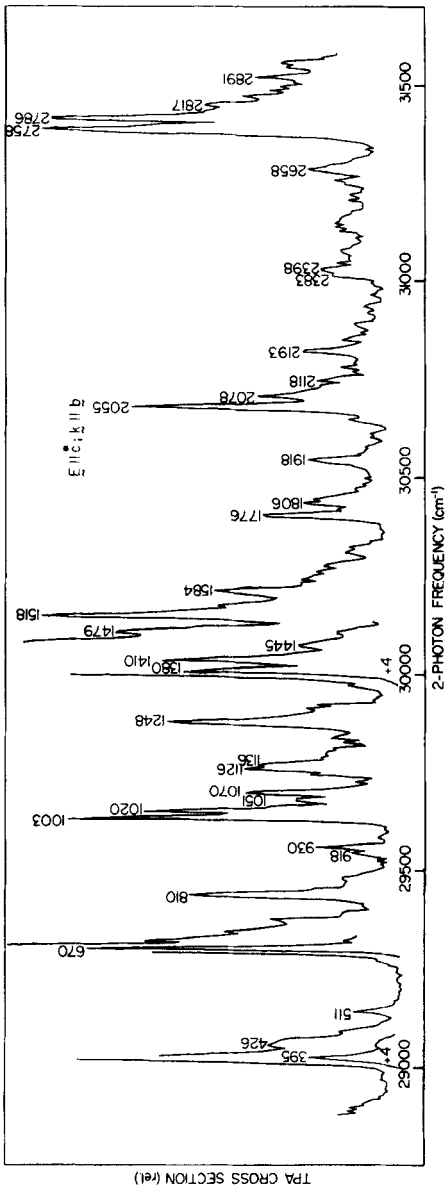


FIGURE 1 **b**(**c***) polarized two-photon excitation spectrum of phenanthrene at $T \sim 6$ K showing the frequency region from 394 $cm^{-1}$ to higher energy. **b** is the propagation vector, perpendicular to the *ac* face.(**c***) defines the polarization of the two absorbed photons (see text). Peaks are labeled relative to 29,627 $cm^{-1}$, the midpoint between the zero-point lower and upper Davydov components as reported by Craig and Gordon.

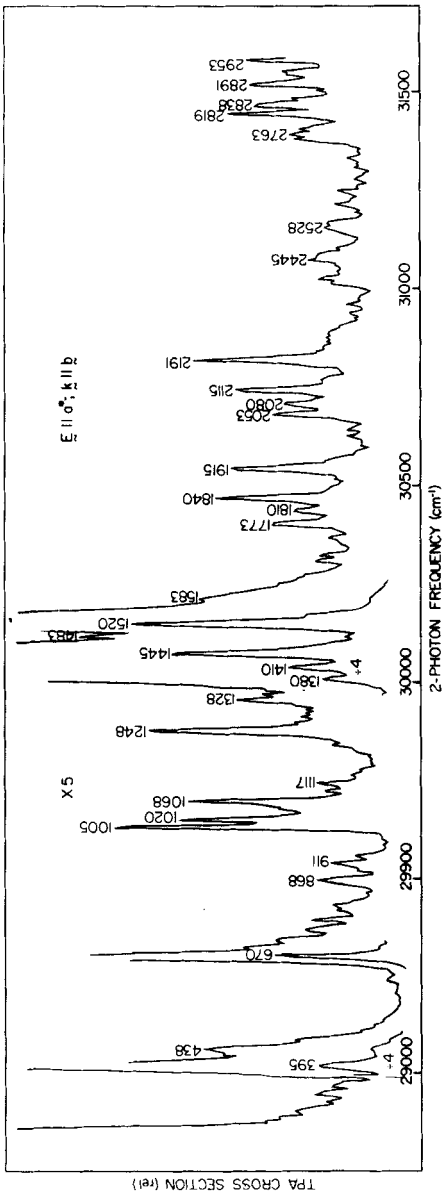


FIGURE 2 **b(a*a*)** TPE spectrum of phenanthrene at $T \sim 6$ K showing the frequency region from 394 $cm^{-1}$ to higher energy. Cf. caption to Figure 1.

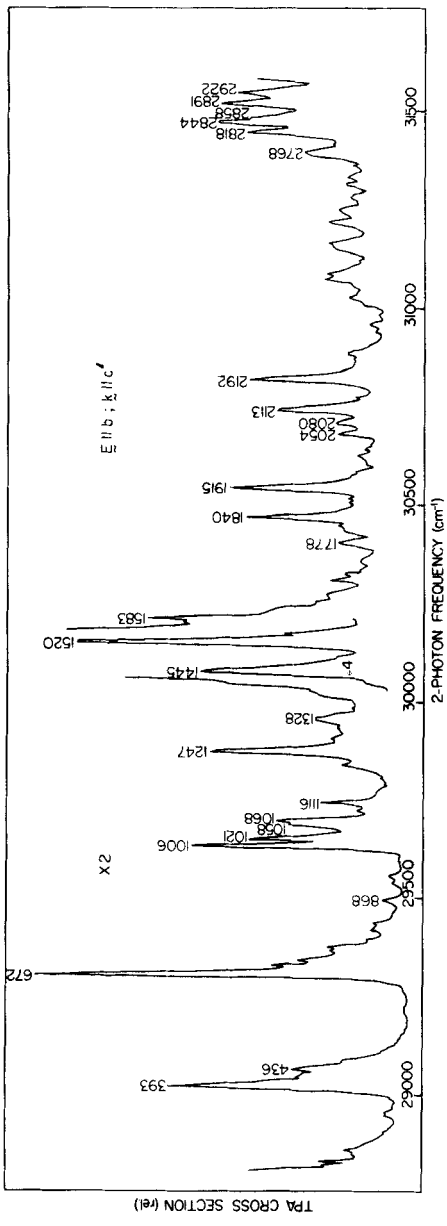


FIGURE 3 c'(bb) TPE spectrum of phenanthrene at $T \sim 6$ K showing the frequency region from 394 $cm^{-1}$ to higher energy. Cf. caption to Figure 1.

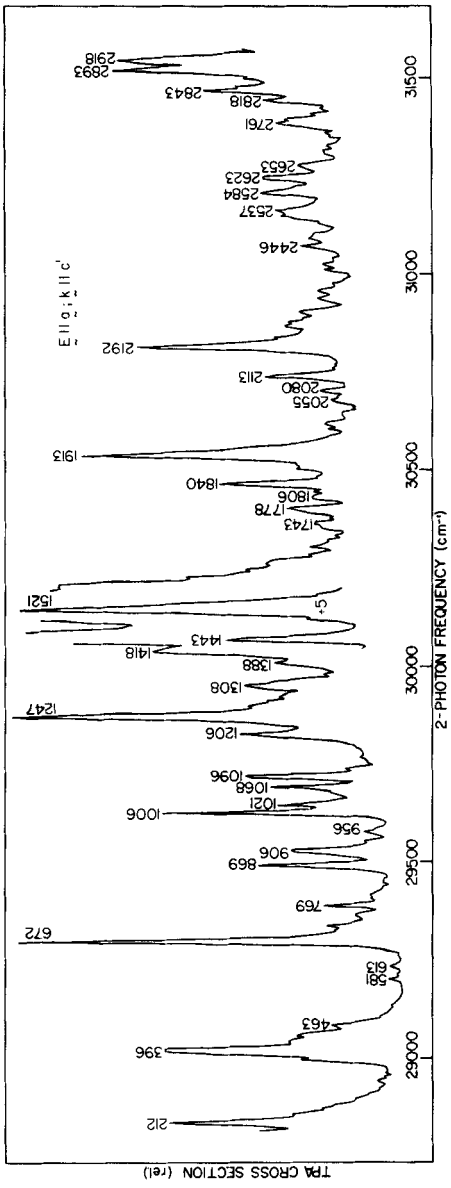


FIGURE 4 c'(**aa**) TPE spectrum of phenanthrene at $T \sim 6$ K showing the frequency region from 394 $cm^{-1}$ to higher energy, Cf. caption to Figure 1.

with nontotally symmetric vibrations or phonon side bands building on zero-phonon vibronic bands will be discussed in a future paper. With this in mind, Table III lists the vibrational frequencies along with assignments. The former are averages for at least two spectra and are, within experimental error ($\pm 2\,cm^{-1}$), independent of polarization or **K**. Also included in Table III are intensities measured relative to the upper Davydov component origin $O_U$ assigned an arbitrary intensity of 100 for each polarization (diagonal). Using the NPDL, it was found that the *integrated* intensity ratio of the $394\,cm^{-1}$ band relative to $O_U$ is, within experimental error, the same for **b(a*a*)**, **b(c*c*)**, and **c*(bb)**—slightly greater than 0.30. A rounded off intensity value of 30 is used in Table III. Figures 1–4 and additional spectra were then used to measure average values for the peak heights of other vibronic bands relative to the peak height of the $394\,cm^{-1}$ fundamental. These relative peak heights appear in Table III with one exception: the linewidth of the $672\,cm^{-1}$ fundamental was always found to be about half that of the $394\,cm^{-1}$ band (*ca.* 9 vs. $18\,cm^{-1}$) and thus the intensities for $672\,cm^{-1}$ listed in Table III are reduced by a factor of 2 relative to their peak height values.

The vibronic structure and intensities in Figures 1–4 are discussed in the following section but it is instructive at this point to make some general observations. First, the **b(c*c*)** spectrum, Figure 1, bears the closest resemblence to Craig and Gordon's one-photon absorption spectrum[7] (**K** perpendicular to the *ab* face) in that the $a_1$ fundamentals 672, 1380 and $1410\,cm^{-1}$ dominate the vibrational structure. The overtone of $1380\,cm^{-1}$ appears strongly as $2760\,cm^{-1}$ followed by the combination band 1380 and $1410\,cm^{-1}$, Table III. The 394 and $672\,cm^{-1}$ fundamentals form prominent combinations with both the 1380 and $1410\,cm^{-1}$ bands. Since the one-photon absorption spectrum[7,8] exhibits little vibronic activity except that which has been proposed[7,8,10] for the $672\,cm^{-1}$ band, one can assert that the **b(c*c*)** spectrum is similarly of a Franck–Condon type. This is consistent with our polarization intensity ratio measurements for $O_U$ and $394\,cm^{-1}$ which yield **b(c*c*)**: **b(a*a*)** $\sim 5$ and **c*(bb)**:**c*(a*a*)** $\sim 2$. The direction cosines in Table I show that these ratios are consistent with $B_2$(L) molecular states playing a dominant role as intermediate states (vide infra). In the **b(a*a*)**, **c′(aa)** and **c′(bb)** spectra, Figures 2–4, very interesting intensity changes occur in the 1380–$1520\,cm^{-1}$ region since now the 1444 and $1520\,cm^{-1}$ $a_1$ fundamentals dominate the 1380 and $1410\,cm^{-1}$ bands. In particular, referring to Figure 4 and Table III, one observes that the former two bands are more intense than the origin $O_U$ while the overtone of $1444\,cm^{-1}$ and the combination of $1444 + 1520\,cm^{-1}$ are far less intense than predicted in the Condon approximation. It will be argued later that these two fundamentals are vibronically active.

Ito *et al.*[17] reported earlier the **c′(bb)** TPE spectrum for phenanthrene at 4.2 K and stated that this spectrum differs little from the **c′(aa)** spectrum. In

TABLE III

Vibrational analysis for the TPE spectra of the 350 nm system of phenanthrene

| 2-photon $cm^{-1}$ [a] | Interval from 28,627 $cm^{-1}$ [b] | Intensity[c] $a^*a^*$ | $bb$ | $c^*c^*$ | Assignment |
|---|---|---|---|---|---|
| | | 100 | | | $O_U$[d] |
| | | | 1000 | | $O_U$[d] |
| | | | | 100 | $O_U$[d] |
| 28,842 | 215 | 2 | — | <1 | $f(a_1)$ |
| 29,021 | 394 | 30 | 30 | 30 | $f(a_1)$ |
| 29,138 | 511 | <1 | — | 3 | $f$ |
| 29,299 | 672 | 30 | 30 | 50 | $f(a_1)$ |
| 29,437 | 810 | ~1 | sh, ~2 | 15 | $f(a_1)$ |
| 29,496 | 869 | 4 | 3 | sh, ~1 | ? |
| 29,539 | 912 | 3 | 1 | 3 | ? |
| 29,557 | 930 | 2 | 2 | 5 | ? |
| 29,632 | 1005 | 20 | 30 | 25 | $f$ |
| 29,647 | 1020 | 15 | 20 | 20 | $f(a_1)$ |
| 29,678 | 1051 | sh, ~1 | — | 7 | ? |
| 29,695 | 1068 | 10 | 15 | 12 | 394 + 672 |
| 29,723 | 1096 | 3 | sh, 3 | 2 | ? |
| 29,743 | 1116 | 3 | 9 | sh, ~3 | $f(a_1)$ |
| 29,753 | 1126 | — | — | ~10 | $f$ |
| 29,837 | 1210 | sh, ~1 | sh, ~4 | 3 | $f(a_1)$ |
| 29,875 | 1248 | 15 | 25 | 20 | $f(a_1)$ |
| 29,955 | 1328 | 8 | 8 | — | $f(a_1)$ |
| 29,969 | 1342 | sh, ~2 | — | sh, ~2 | 2 × 672 |
| 30,007 | 1380 | 25 | sh, ~5 | 70 | $f(a_1)$ |
| 30,037 | 1410 | 40 | sh, ~5 | 75 | $f(a_1)$ |
| 30,071 | 1444 | 90 | 120 | 30 | $f(a_1)$ |
| 30,104 | 1479 | sh, ~8 | sh, ~6 | sh, ~10 | 672 + 810 |
| 30,145 | 1518 | 90 | 180 | 25 | $f(a_1)$ |
| 30,210 | 1583 | sh, ~4 | ~20 | 10 | $f(a_1)$ |
| 30,307 | 1680 | 3 | 6 | 3 | 672 + 1005 |
| 30,321 | 1694 | 3 | 3 | 3 | 672 + 1020 |
| 30,402 | 1775 | 5 | 5 | 10 | 394 + 1380 |
| 30,433 | 1806 | 3 | sh, ~4 | 6 | 394 + 1410 |
| 30,467 | 1840 | 10 | 15 | sh, 2 | 394 + 1444 |
| 30,542 | 1915 | 10 | 20 | 5 | 394 + 1518 |
| 30,681 | 2054 | 5 | 4 | 30 | 672 + 1380 |
| 30,707 | 2080 | 5 | 4 | 15 | 672 + 1410 |
| 30,742 | 2115 | 10 | 15 | 5 | 672 + 1444 |
| 30,819 | 2192 | 10 | 20 | 10 | 672 + 1518 |
| 31,010 | 2383 | 3 | sh, ~2 | ~3 | 1005 + 1380 |
| 31,028 | 2401 | 3 | 4 | ~3 | 1020 + 1380 |
| 31,073 | 2446 | ~3 | 7 | ~2 | 1005 + 1444; 1068 + 1380 |
| 31,089 | 2462 | 3 | 7 | — | 1020 + 1444 |
| 31,153 | 2526 | 3 | 7 | ? | 1005 + 1518 |
| 31,167 | 2540 | 3 | 7 | ? | 1020 + 1518 |
| 31,211 | 2584 | 2 | 6 | ~1 | 1068 + 1520 |
| 31,250 | 2623 | 2 | 4 | 2 | 1248 + 1380 |
| 31,282 | 2655 | 1 | 3 | 5 | 1248 + 1410 |

TABLE III—*continued*

| 2-Photon $cm^{-1}$ [a] | Interval from 28,627 $cm^{-1}$ [b] | Intensity[c] $a^*a^*$ | $bb$ | $c^*c^*$ | Assignment |
|---|---|---|---|---|---|
| 31,315 | 2688 | 1 | 4 | — | 1248 + 1444 |
| 31,387 | 2760 | ~4 | sh, ? | 20 | 2 × 1380 |
| 31,398 | 2771 | | 9 | sh, ? | 1248 + 1518 |
| 31,412 | 2785 | sh, ~1 | — | 20 | 1380 + 1410 |
| 31,444 | 2817 | 8 | 15 | ~10 | 2 × 1410; 1380 + 1445 |
| 31,469 | 2842 | 6 | 20 | sh, ~5 | 1410 + 1444 |
| 31,518 | 2891 | 6 | 20 | 7 | 2 × 1444 |
| 31,540 | 2913 | 3 | ~15 | 5 | 1410 + 1518 |
| 31,585 | 2955 | 6 | 15 | — | 1444 + 1518 |

[a] Vacuum corrected. See Figures 5–8 for upper Davydov component regions **b(c*c*)**, **b(a*a*)**, **c*(bb)**, **c*(a*a*)**

[b] 28,627 $cm^{-1}$ is the midpoint between the upper and lower Davydov components measured by Craig and Gordon, Ref. (7).

[c] See text, section iv, for explanation of relative intensities.

[d] The location and profile of the upper Davydov component region depends on **k** and polarization, see footnote a.

both, the 1380, 1410, 1444 and 1520 $cm^{-1}$ fundamentals are barely resolved (their reported linewidths are *ca.* 3 × those reported here) but appear to have equal intensity in contrast with our data. Our measurements have been repeated on several crystals and with two different laser/detection systems and in all cases the 1380 and 1410 $cm^{-1}$ bands are weak relative to 1444 and 1520 $cm^{-1}$. From Table III one observes that the former two fundamentals carry only 5% the intensity of $O_U$ and are even weaker relative to the latter two fundamentals for **c'(bb)**. We do not understand why the linewidths of Ito *et al.* are so broad relative to ours. They do speculate that the 1444 and 1520 $cm^{-1}$ are vibronically active but offer no spectroscopic data nor calculations which support this contention. We turn our attention now to the origin region.

This region for **b(c*c*)**, **b(a*a*)**, **c*(bb)** and **c*(a*a*)** appears in Figures 5–8, respectively. One is immediately struck by the **K**- and polarization-dependence of the "upper" component. For example, the center of gravity of this component (measured relative to the lower Davydov component at 28597 $cm^{-1}$) shifts to higher energy by about 60 $cm^{-1}$ in going from **b(c*c*)** to **c*(bb)** and there are marked structural changes as well. One should also note the differences between the **c*(bb)** and **c*(a*a*)** spectra. In the static lattice approximation one does not expect to observe the lowest Davydov component, *vide supra*, consistent with Figures 5, 7 and 8. The unexpected intensity of $O_L$ in Figure 6 is almost certainly due to imperfect cutting of the *ac* section and misalignment since in more recently obtained **b(a*a*)** spectra the

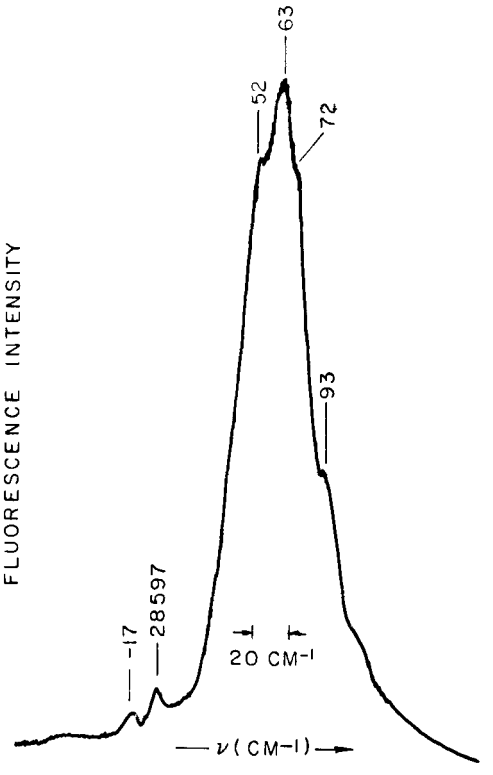


FIGURE 5 Origin region of the **b(c*c*)** polarized two-photon excitation spectrum of phenanthrene at $T \sim 6$ K. (The notation for the polarization and propagation vectors is explained in the caption to Figure 1.) Relative frequencies are measured from 28,597 $cm^{-1}$, the frequency of the lower Davydov component.

intensity of $O_L$ relative to $O_U$ is diminished by a factor of $\sim 3$. The lowest Davydov component for **K** perpendicular to a principal section and crossed polarization is formally allowed. In Figure 9 appears the **c*(a*b)** spectrum. The spectrum is a summation of the two spectra in Figures 7 and 8 plus the cross-polarization spectrum which derives from the two photons absorbed having mutually orthogonal polarization. The cross-polarization component is responsible for the appearance of $O_L$ at 29597 $cm^{-1}$.

The **b(a*c*)** spectrum in Figure 10 is to be compared with those of Figures 5 and 6. As the theory predicts, cf. section II, no cross-polarization TPA is allowed for **b(a*c*)** consistent with Figures 5, 6 and 10 and the fact that the **b(c*c*)** spectrum is *ca.* 5 × more intense than **b(a*a*)**, *vide supra.*

Thus, while the so-called upper component undergoes the aforementioned center of gravity shift with **K** and polarization, the lower component remains fixed in absolute energy *along* with the vibronic bands. In addition to the spectra in Figures 5–10, we have also measured the **a*(bb)** and **a*(c*c*)** origin

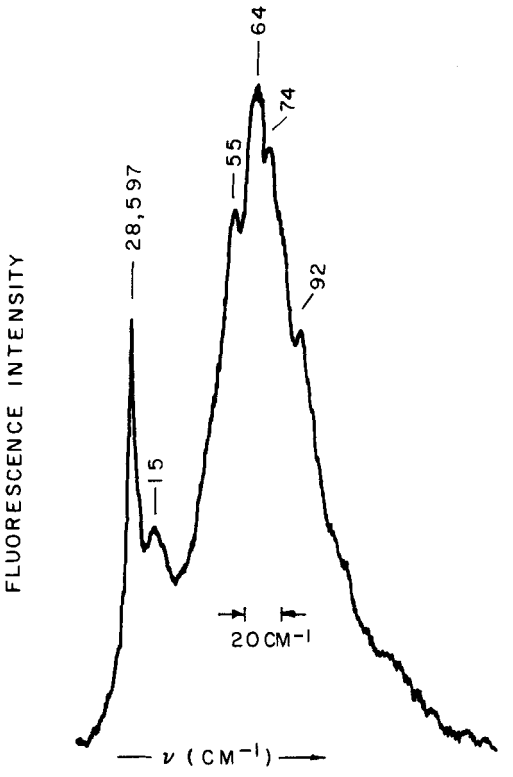


FIGURE 6 Origin region of the b(a*a*) TPE spectrum of phenanthrene at $T \sim 6$ K. Cf. caption to Figure 5.

regions. The lower Davydov component is observed very weakly and for the former spectrum the center of gravity of the upper component agrees well with that in Figure 7. For the latter spectrum the upper component is *ca.* twice as broad as it appears in Figure 5 and located at $\sim 90\,\mathrm{cm}^{-1}$. The problem of understanding the **K** and polarization dependence of the upper component is intriguing. Three explanations which we consider in section VI are based on exciton-phonon coupling, exciton spatial dispersion and second harmonic generation (SHG).

## V. RESONANTLY DRIVEN SECOND HARMONIC GENERATION

As emphasized by Mahr[11] two-photon resonantly driven SHG from the term

$$\sum_n \left\{ \frac{\langle g|r_i|n\rangle\langle n|r_j|m\rangle\langle m|r_k|g\rangle}{(\omega_{ng} - \omega_1)(\omega_{mg} - \omega_3)} \right\} \tag{4}$$

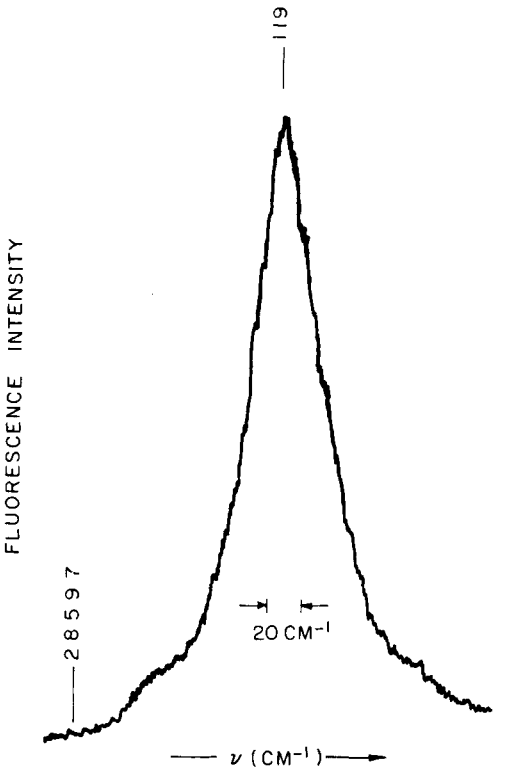


FIGURE 7 Origin region of the **c*(bb)** TPE spectrum of phenanthrene at $T \sim 6$ K. Cf. caption to Figure 5.

in the third order electric dipole susceptibility can be experimentally mistaken for TPA. This follows since $\omega_3 = \omega_1 + \omega_2$, the sum of the incident photon frequencies so that $\omega_{mg} - \omega_3$ represents a two-photon resonance. In Eq. (4) $|g\rangle$ is the ground state while $|n\rangle$ and $|m\rangle$ are intermediate states. The $r_i$ are components of the electric dipole moment operator **d**. The SHG wave can be absorbed by the solid resulting in incoherent fluorescence indistinguishable from that produced by TPA— Hochstrasser and Meredith[1] in their studies of the lowest singlet exciton level of naphthalene and anthracene have taken advantage of SHG to probe the polariton dispersion curves. The situation in these systems is different from ours since their TPA and resonantly driven SHG are formally forbidden in the electric dipole approximation. For the phenanthrene exciton levels of interest here both are in general dipole allowed. However, for the incident direction **K** of the transverse photons parallel to the screw axis **b**, as is the case for our **b(a*a*)** and **b(c*c*)** spectra, SHG is forbidden (static lattice approximation). This follows from (4) noting

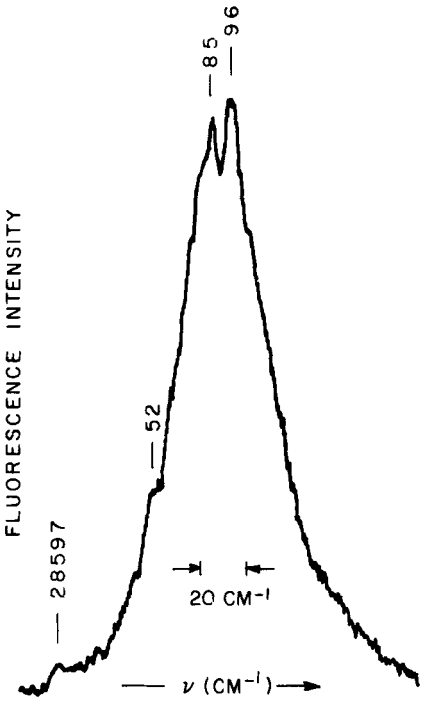


FIGURE 8 Origin region of the **c*(a*a*)** TPE spectrum of phenanthrene at $T \sim 6$ K. Cf. caption to Figure 5.

that for the group of the wavevector $\cong C_2$ we have the reps $\Gamma(r_k) = \Gamma(r_j) = B$ and, of course $\Gamma(|g\rangle) = A$. Thus, the integrand of (4) vanishes unless $\Gamma(r_i) =$ $\Gamma$(electric vector of the SHG wave) $= A$ which means that the SH wave is polarized parallel to its propagation direction **b** (i.e. longitudinal). It is impossible to generate such a wave since in the dipole approximation the interaction hamiltonian depends only on the electric field strength parallel to the transverse vector potential.

Similar arguments show, however, that SHG can occur for phenanthrene when **K** is perpendicular to **b** and thus could represent an interference in our **c*(a*a*)** and **c*(bb)** spectra for example. We first consider whether strong phase matching for SHG, i.e. $n_\omega = n_{2\omega}$, could develop in the vicinity of the upper Davydov component $O_U$. That is, is this isolated component's oscillator strength sufficiently strong to introduce strong temporal dispersion for the real part of the refractive index $n$ near its resonance energy? To this end a simple calculation for an isotropic medium with dielectric constant

$$\varepsilon(\omega) = \varepsilon_0 - \frac{f^2/2\omega}{\omega - \Omega r + i\gamma} \tag{5}$$

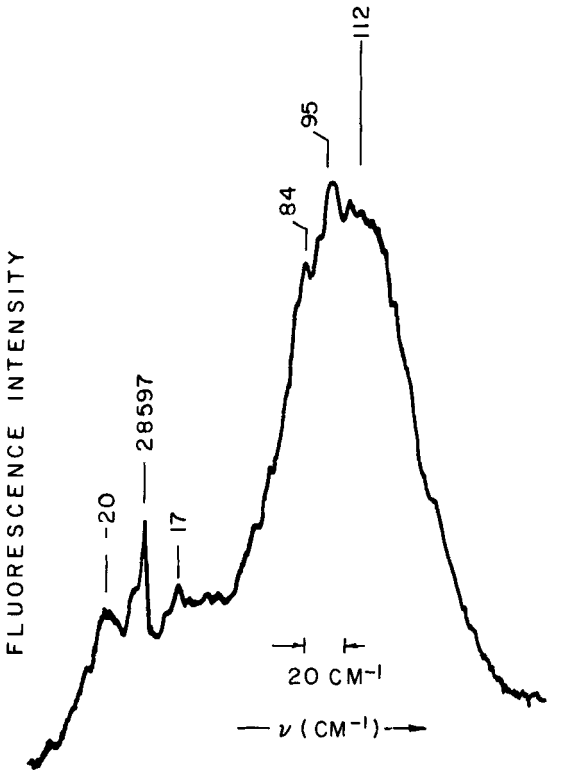


FIGURE 9 Origin region of the **c*(a*b)** TPE spectrum of phenanthrene at $T \sim 6$ K. The spectrum is a summation of the spectra in Figures 7 and 8 plus the cross-polarized spectrum due to the absorption of two photons having mutually orthogonal polarization.

suffices. $\varepsilon_0$ is the dielectric constant due to the background states, $\Omega_r$ is the isolated resonance frequency (spatial dispersion can be safely neglected) and $\gamma$ is the damping constant of the exciton level. The term $f^2$ is proportional to the oscillator strength

$$f^2 = \frac{4\pi^2 e^2}{m} \frac{F}{V} \tag{6}$$

where $F/V$ is the volume density of the oscillator strength. The real ($\varepsilon'$) and imaginary ($\varepsilon''$) parts of $\varepsilon$ are obtained from Eq. (5) and related to the refractive index $N = n + i\kappa$ using

$$\varepsilon' = n^2 - \kappa^2; \qquad \varepsilon'' = 2n\kappa. \tag{7}$$

Provided the solution value for the oscillator strength of the 350 nm absorp-

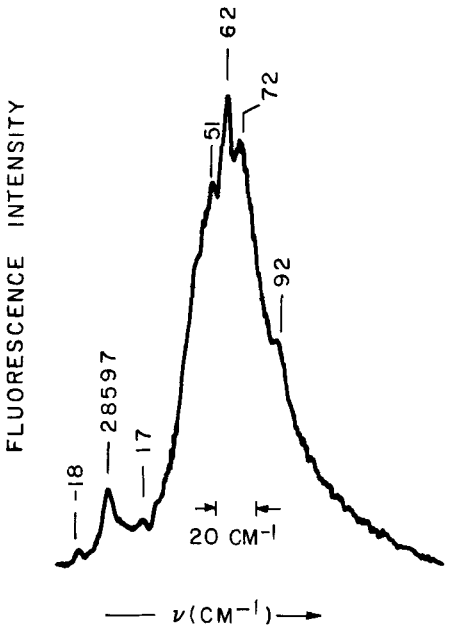


FIGURE 10 Origin region of the b(a*c*) TPE spectrum of phenanthrene at $T \sim 6$ K. The spectrum is a summation of the spectra in Figures 5 and 6.

tion system equal to $\sim 10^{-3\,7}$ is transferable to the crystal as a reasonable estimate for the oscillator strength of the upper Davydov component (treated as a single oscillator) is $3 \times 10^{-4}$. For $\gamma$ we choose $10\,\text{cm}^{-1}$ judged to be reasonable because the dephasing of the upper component due to phonon emission processes to the lower exciton branch is expected to be fast. This value of $\gamma$ is about a factor of 2 smaller than the value reported by Syassen and Philpott.[9] Our calculation ($\varepsilon_0 = 3.5$) of $n(\omega)$ shows that the isolated resonance due to the upper Davydov component perturbs $n_0 = \varepsilon_0^{1/2}$ only slightly ($< 1\,\%$). On this basis one expects no strong SHG phase matching in the vicinity of $O_U$ or any of the weaker vibronic features so that if *resonantly* driven SHG is competitive with TPA the former should exhibit a frequency profile very similar to that for TPA.[11] However, our calculation can only be considered instructive since Syassen and Philpott[9] observe a fairly pronounced reflectivity peak corresponding to $O_U$ with $\mathbf{K} \perp ab$. The oscillator strength of $3 \times 10^{-4}$ used in our calculation is too small to account for their data. Indeed for their single oscillator fit of the reflection peak (see section VI for further discussion) Syassen and Philpott employ an oscillator strength of $\sim 3 \times 10^{-2}$ which is difficult to reconcile since it is more than an order of magnitude greater than the solution value for the *entire* absorption system.

Nevertheless, the reflection spectrum which for $O_U$ at 1.5 K shows a reflectivity maximum and minimum of *ca.* 16% and 6%, respectively, cannot be disputed. The calculation of $n(\omega)$ was repeated with $F = 3 \times 10^{-2}$ and $\gamma = 10\,\text{cm}^{-1}$. Noting that $n_0 = 1.87$ we calculate a maximum value of $n = 2.5$ ($\sim 10\,\text{cm}^{-1}$ to lower energy of the exciton resonance) and a minimum value of $n = 1.3$ (lying $\sim 15\,\text{cm}^{-1}$ to higher energy of the resonance). The functional behavior of $n(\omega)$ is of the normal type.[18]

For the **c*(bb)** and **c*(a*a*)** orientations the outgoing SH waves propagating along **c*** should both be polarized parallel to **b**. At $\lambda = 546\,\text{nm}$ $n_{a^*} = 1.55$ and $n_b = 1.72$ and the above calculation shows that strong phase matching could occur for both cases in the range $\approx 5$–$8\,\text{cm}^{-1}$ to higher energy of the upper Davydov component resonance. For **c*(a*a*)** an additional phase matching at $\approx 35\,\text{cm}^{-1}$ to higher energy of the resonance is also possible. In the third part of the following section, however, arguments against SHG playing an important role in the **c*(bb)** and **c*(a*a*)** spectra are presented. The first two parts of the section deal with the vibronic structure analyses, the essential features of which can be determined from the **b(c*c*)** and **b(a*a*)** spectra where no complications due to SHG are anticipated, *vide supra.*

## VI. DISCUSSION

### Symmetry of dominant intermediate states

The symmetries of the $\pi\pi^*$ molecular electronic states which can serve as virtual states in TPA to the 350 nm $^1A_1$ state are $A_1$(M) and $B_2$(L). For **K**$\|$**b** our data show that the intensity ratio $I_{c^*c^*}:I_{a^*a^*} \approx 5$ for the upper Davydov component $O_U$. For **K** $\|$ **c*** $I_{bb}:I_{a^*a^*} \approx 2$. These *diagonal* polarization ratios together with the oriented gas ratios in Table II indicate that intermediate states of $B_2$ symmetry are most effective in TPA. It is instructive to consider whether a simple Hückel MO calculation supports this experimental finding. To this end we can employ the Condon approximation to write, *vide infra.*

$$M_{Ff \leftarrow Go} = \langle f|0\rangle \sum_I [E_I - E_1]^{-1}(\boldsymbol{\varepsilon}_2 \cdot \mathbf{D}_{FI})(\boldsymbol{\varepsilon}_1 \cdot \mathbf{D}_{IG}) + d_{1\leftrightarrow 2} \qquad (8)$$

for the two-photon matrix element corresponding to the transition $Ff \leftarrow Go$. Here $F$ and $f$ denote the electronic and vibrational states, respectively, while $I$ labels the electronic intermediate state. The **D** vectors are electronic transition dipoles. $\boldsymbol{\varepsilon}_2$ and $\boldsymbol{\varepsilon}_1$ are the polarizations of the two photons and $d_{1\leftrightarrow 2}$ is obtained from the first term in the summation by interchanging indices

1 and 2. $E_I$ and $E_1$ are the energies of the intermediate electronic state and photon "1", respectively. Intensity is proportional to $|M_{Ff\leftarrow Go}|^2$. We consider two cases: $\varepsilon_1, \varepsilon_2 \| \mathrm{L}$ and $\varepsilon_1, \varepsilon_2 \| \mathrm{M}$ so that the electronic part of Eq. (8) becomes

$$M_{F\leftarrow G} = 2\sum_I [\omega_I - \omega_1]^{-1} \mathbf{D}_{FI} \cdot \mathbf{D}_{IG} \tag{9}$$

The key point to recognize is that for intermediate states $I$ of a given symmetry their transition dipoles, e.g. $\mathbf{D}_{FI}$, are either parallel or anti-parallel so that interferences can arise in $\sum_I$. The difficulty in evaluating $M_{F\leftarrow G}$ for phenanthrene is that accurate LCAO SCF CI wavefunctions for all $\pi\pi^*$ states are not available. Such wavefunctions would, in any event, be difficult to generate accurately, especially for the higher lying states. However, a reasonably accurate approach is to employ the singly excited, excited state configurations themselves with neglect of CI realizing that since in Eq. (9) we sum over all possible states the error introduced through neglect of CI is minimized due to averaging.[19] This we have done using the Hückel $\pi$ MOs[20] for phenanthrene and find that[21]

$$\left|\sum_I \mathbf{D}_{FI} \cdot \mathbf{D}_{IG}\right| = 0.07 \text{ Å}^2 \text{ and } 0.84 \text{ Å}^2$$

for $I = A_1$ and $B_2$, respectively. For the former case the principal configurations by and large destructively interfere, while for the latter case they constructively interfere. In our opinion these interferences would not be reversed by a highly refined computation. Thus, the calculation is taken to be supportive of the experimental finding that the Condon part of the TPA to the 350 nm state of phenanthrene is dominated by intermediate states of $B_2$ symmetry. Importantly, this is consistent with the fact that the **b(c*c*)** spectrum, Figure 1, showing the dominance of the 1380 and 1410 $\mathrm{cm}^{-1}$ fundamentals, is very similar to the Condon-like one-photon spectrum of Craig and Gordon[7] in contrast with the **b(a*a*)**, **c′(bb)** and **c′(aa)** spectra, Figures 2–4.

These facts together with the **b(c*c*)** relative vibronic intensities in Table III indicate that Figure 1 is by and large a Franck–Condon (FC) spectrum. For example, taking the ratios of the fundamental intensities relative to $O_U$ (Table III) as the FC factors for the fundamentals 392, 672, 1380, 1410 and 1518 one finds that the calculated intensities of the combinations they form with each other are in reasonable agreement with the observed values (the latter generally $\sim \times 2$ too weak). Differences of this magnitude are expected since the relative intensities in Table III are for peak heights. The intensity of $2 \times 1380$ relative to the fundamental leads to a value of the FC factor parameter $D = 1.08$[22] which leads to a FC factor for the 1380 $\mathrm{cm}^{-1}$ fundamental equal to 0.6. This value is in good agreement with the value of 0.7

obtained from Table III. While we do not exclude the possibility that some of the $a_1$ fundamentals are to a small extent vibronically active in the **b(c*c*)** spectrum, we feel that the bulk of this spectrum is explicable within the framework of the Condon approximation. The one exception seems to be the 672 $cm^{-1}$ fundamental. For if one assumes it is a FC mode its FC factor of 0.5 leads to a predicted intensity of 13 for $2 \times 672 = 1344\ cm^{-1}$. A weak band at 1342 $cm^{-1}$ is observed but with an intensity of only 2, Table III. This situation is similar to that in the one-photon spectrum where Craig and Small[10] have concluded that the 672 $cm^{-1}$ mode is both Herzberg–Teller (HT) and FC active. It is a relatively simple matter to show that this situation is not altered in the TPA spectrum when the intermediate states are of $B_2$ symmetry. Thus, it is likely that for the **b(c*c*)** spectrum the 672 $cm^{-1}$ $a_1$ fundamental is vibronically active.

For the purpose of discussing the vibronic structure in Figures 2–4 we need an expression for the TPA matrix element $M_{Ff\leftarrow Go}$ which includes the vibronic coupling contribution. One can show that

$$\begin{aligned} M_{Ff\leftarrow Go} = \sum_{Ii} [E_{Ii} - E_1]^{-1} \Big\{ & (\boldsymbol{\varepsilon}_2 \cdot \mathbf{D}_{FI})(\boldsymbol{\varepsilon}_1 \cdot \mathbf{D}_{IG}) \langle f | i \rangle \langle i | 0 \rangle \\ & + \sum_{J \neq G} V_{JG} (\boldsymbol{\varepsilon}_2 \cdot \mathbf{D}_{FI})(\boldsymbol{\varepsilon}_1 \cdot \mathbf{D}_{IJ}) \langle f | i \rangle \left\langle i \left| Q - \frac{\hbar^2 \, \partial/\partial Q}{E_G - E_J} \right| 0 \right\rangle \\ & + \sum_{J \neq I} V_{IJ} (\boldsymbol{\varepsilon}_2 \cdot \mathbf{D}_{FI})(\boldsymbol{\varepsilon}_1 \cdot \mathbf{D}_{JG}) \langle f | i \rangle \left\langle i \left| -Q - \frac{\hbar^2 \, \partial/\partial Q}{E_I - E_J} \right| 0 \right\rangle \\ & + \sum_{J \neq I} V_{JI} (\boldsymbol{\varepsilon}_2 \cdot \mathbf{D}_{FJ})(\boldsymbol{\varepsilon}_1 \cdot \mathbf{D}_{IJ}) \left\langle f \left| Q - \frac{\hbar^2 \, \partial/\partial Q}{E_I - E_J} \right| i \right\rangle \langle i | 0 \rangle \\ & + \sum_{J \neq F} V_{FJ} (\boldsymbol{\varepsilon}_2 \cdot \mathbf{D}_{JI})(\boldsymbol{\varepsilon}_1 \cdot \mathbf{D}_{IG}) \left\langle f \left| -Q - \frac{\hbar^2 \, \partial/\partial Q}{E_F - E_J} \right| i \right\rangle \langle i | 0 \rangle \Big\} \\ & + d_{1 \leftrightarrow 2} \end{aligned} \tag{10}$$

is the appropriate expression. The first term in curly brackets derives from the Condon approximation while the last four derive from both adiabatic and nonadiabatic vibronic coupling. We have omitted the summation over all normal coordinates $Q$. The vibronic coupling matrix element $V_{MN} = \langle M | \partial N/\partial Q \rangle\, Q = 0$ where, e.g., $| M \rangle$ is the electronic wavefunction for state $M$. The $Q$ and $\partial/\partial Q$ components of the vibrational matrix elements correspond to the HT and nonadiabatic types of vibronic coupling. Eq. (10) includes them through ground state, final state and intermediate state vibronic coupling with the $J$ states. It is, however, too complicated for vibronic analysis so we simplify by assuming that the vibrational energy contribution to the vibronic energy $E_{Ii}$ is small relative to the electronic energy gaps so

that $E_{Ii} \approx E_I$. With this assumption Eq. (10) takes the form

$$M_{Ff \leftarrow Go} = \sum_I [E_I - E_1]^{-1} \Big\{ (\boldsymbol{\varepsilon}_2 \cdot \mathbf{D}_{FI})(\boldsymbol{\varepsilon}_1 \cdot \mathbf{D}_{IG}) \langle 1 | 0 \rangle + \sum_{J \neq G} V_{JG} (\boldsymbol{\varepsilon}_2 \cdot \mathbf{D}_{FI})(\boldsymbol{\varepsilon}_1 \cdot \mathbf{D}_{IJ}) \left\langle f \left| Q - \frac{\hbar^2 \partial/\partial Q}{E_G - E_J} \right| 0 \right\rangle + \sum_{J \neq I} V_{IJ} (\boldsymbol{\varepsilon}_2 \cdot \mathbf{D}_{FI})(\boldsymbol{\varepsilon}_1 \cdot \mathbf{D}_{JG}) \left\langle f \left| -Q - \frac{\hbar^2 \partial/\partial Q}{E_I - E_J} \right| 0 \right\rangle + \sum_{J \neq I} V_{JI} (\boldsymbol{\varepsilon}_2 \cdot \mathbf{D}_{FJ})(\boldsymbol{\varepsilon}_1 \cdot \mathbf{D}_{IG}) \left\langle f \left| Q - \frac{\hbar^2 \partial/\partial Q}{E_I - E_J} \right| 0 \right\rangle + \sum_{J \neq F} V_{FJ} (\boldsymbol{\varepsilon}_2 \cdot \mathbf{D}_{FI})(\boldsymbol{\varepsilon}_1 \cdot \mathbf{D}_{IG}) \left\langle f \left| -Q - \frac{\hbar^2 \partial/\partial Q}{E_F - E_I} \right| 0 \right\rangle \Big\} + d_{1 \leftrightarrow 2}, \quad (11)$$

where now all vibrational integrals involve only the ground and final electronic states. With this equation one sees that in the absence of vibronic coupling (all $\sum_J$ terms = 0) the intramolecular vibrational intensity distribution should be independent of polarization. Comparison of Figures 2–4 with Figure 1 shows that this is not the case so that vibronic coupling effects in the former spectra must be important.

### Intramolecular vibronic coupling

The facts that the *MM* TPA mechanism is, by virtue of interferences, only weakly Condon allowed relative to the *LL* mechanism, *vide supra*, and that the projections of the *L* axis onto the **a***(**a**) and **b** crystallographic axes are so small, Table I, are consistent with the proposal that the **b**(**a***a**), **c**′(**aa**) and **c**′(**bb**) spectra exhibit marked manifestations of vibronic coupling. The essential features of the vibronic coupling can be revealed in all three spectra through a discussion of the **c**′(**bb**) spectrum. In this spectrum we are seeing primarily the contribution of $A_1$ intermediate states to the TPA mechanism, Table I. With reference to the **b**(**c***c**) spectrum one observes in the **c**′(**bb**) spectrum that

i) the $a_1$ fundamentals 1380 and 1410 $cm^{-1}$ are weak relative to the origin $O_U$ and the $a_1$ fundamentals 1444 and 1518 $cm^{-1}$, Table III,

ii) the fundamentals at 1444 and 1518 $cm^{-1}$ are *more* intense than the origin,

iii) the overtone $2 \times 1444$ $cm^{-1}$ and the combination 1444 + 1518 $cm^{-1}$ are considerably less intense than predicted in the Condon approximation,

iv) the combinations of 1380 and 1410 $cm^{-1}$ with the strong 1444 and 1518 $cm^{-1}$ fundamentals are substantially more intense than anticipated in the Condon approximation, Table III.

We are unable to explain (i)–(iv) in a convincing fashion unless we postulate that the TPA matrix elements associated with all four of the $a_1$ fundamentals are comprised of both a FC and vibronic coupling contribution. In this way we can qualitatively understand the vibronic intensities associated with the 1380, 1410, 1444 and 1518 $cm^{-1}$ fundamentals provided their intensities in the **b(c*c*)** spectrum, Table III, yield directly their Franck–Condon factors and $D^{22}$ parameters, *vide supra*. Denoting these four vibrations as *a*, *b*, *c* and *d* we obtain from the *c*c** intensities that $D_a \sim D_b = 1.2$ and $D_c \sim D_d = 0.8$. Within the harmonic approximation one can use Eq. (11) to write the $M_{Ff \leftarrow Go}$ TPA elements in a more tractable form, e.g.

$$\begin{aligned} M_{F1_a \leftarrow Go} = {} & m^c\langle 1a|0a\rangle\langle 0b|0b\rangle\langle 0c|0c\rangle\langle 0d|0d\rangle \\ & + m_a^V\langle 1a|1a\rangle\langle 0b|0b\rangle\langle 0c|0c\rangle\langle 0d|0d\rangle \\ & + m_b^V\langle 1a|0a\rangle\langle 0b|1b\rangle\langle 0c|0c\rangle\langle 0d|0d\rangle \\ & + m_c^V\langle 1a|0a\rangle\langle 0b|0b\rangle\langle 0c|1c\rangle\langle 0d|0d\rangle \\ & + m_d^V\langle 1a|0a\rangle\langle 0b|0b\rangle\langle 0c|0c\rangle\langle 0d|1d\rangle, \end{aligned} \tag{12}$$

where $m^c$ is the Condon contribution to the electronic part of Eq. (11) and $m_a^V$, for example, is the vibronic coupling contribution to the same for mode *a*. The integral $\langle 1a|0a\rangle$ is the overlap between the one quantum level of mode *a* in the final electronic state and the zero quantum level in the ground state. All vibrational integrals can be evaluated using the aforementioned *D* values and a standard compilation of overlap integrals. The **b*b*** intensities of the four fundamentals relative to the origin were used to determine the $m_i^V$ values. We find that $m_a^V = m_b^V = 1.18\,m^c$; $m_c^V = -0.80\,m^c$ and; $m_d^V = -1.18\,m^c$. With these values the calculated and observed intensities of the four fundamentals are in agreement. The calculated intensities (relative to a value of 100 for the origin) for the 1380 + 1444, 2 × 1444, 1410 + 1518 and 1444 + 1518 $cm^{-1}$ bands are 25, 30, 40 and 80, respectively. The observed values from Table III are ~15, 20, 15 and 15. Within the Condon approximation their predicted intensities are 6, 70, 9 and 216. Thus, the near equality of the intensities of the four bands can be reasonably well understood in terms of the simple vibronic coupling model but cannot be understood in terms of the Condon approximation.

In summary, the TPA spectra of phenanthrene derived principally from $A_1$ intermediate states show clear manifestations of vibronic coupling via $a_1$ fundamentals. Particularly noteworthy are the 1380, 1410, 1444 and 1518

$cm^{-1}$ modes whose electronic TPA matrix elements are comprised of both a Condon and vibronic coupling contribution.

### The origin region of the TPE spectra

The dependences of the center of gravity and profile of the upper Davydov component on the photon wavevector **k** and polarization, Figures 5–8, are particularly interesting. In what follows we consider three possible explanations for this behavior based on (i) exciton spatial dispersion, (ii) strongly phase matched SHG, section V, and (iii) the exciton-phonon interaction.

i) *Exciton spatial dispersion* The calculation of the factor group (Davydov) splittings for molecular crystals is well documented.[24,25] It is important to note that the Ewald–Kornfield[26] technique frequently used to compute dipole-dipole interaction lattice sums required for factor group splitting and exciton spatial dispersion analyses has an inherent non-analyticity which can result in a dependence of the factor group splittings and the factor group component $\mathbf{k} = 0$ energies on **k** (wavevector). These effects appear to be important for the 380 nm system of anthracene[27] whose oscillator strength is two orders of magnitude larger than for the 350 nm state of phenanthrene. For anthracene, $\mathbf{k} = 0$ factor group shifts with **k** as large as a few hundred $cm^{-1}$ are calculated.[27] The question is whether the spatial dispersion can explain the aforementioned shifts of the upper Davydov component. For the **b**(**c***c******) and **b**(**a***a******) spectra, its center of gravity is at *ca.* 64 $cm^{-1}$ relative to $O_L$), Figures 5, 6. For the **c***(**bb**) and **c***(**a***a******) spectra, Figures 7 and 8, the center of gravity lies at *ca.* 120 and 90 $cm^{-1}$, respectively. In the **a***(**bb**) and **a***(**c***c******) spectra (not reproduced here) it lies at *ca.* 120 and 90 $cm^{-1}$, respectively. We consider that the centers of gravity correspond roughly to the zero-phonon transitions associated with the upper component. Now one can exclude spatial dispersion as being solely responsible for these shifts on two grounds: first, the theory of exciton spatial dispersion predicts that for a given principal face the upper Davydov component must have the same energy and therefore its locations for the two polarizations in the TPE experiment must be the same. The data show this not to be the case. Second, if the upper component shifts with **k** sense the zero-phonon lower component should also.[27] In all our spectra the latter appears at the same energy. We note that the factor group splitting for the origin region has been determined from one-photon transmission[7] and reflection[9] spectra obtained with the incident photon direction perpendicular to the *ab* face. Splittings were measured to be 59 and 44 $cm^{-1}$, respectively. These measurements do not agree with Ewald calculations[25] which predict a much reduced splitting, 8 $cm^{-1}$, *for the entire* absorption system and also err in the direction of the splitting. Our calcula-

tion of $\mathbf{k} = 0$ splitting within this simple model predicts that it should be greatest for $\mathbf{k} \| \mathbf{b}$ with, for example, the $\mathbf{k} \| \mathbf{c}'$ splitting smaller by a factor of 6.8. Scaling of the transition dipole associated with the origin will not alter this situation which is inconsistent with a model where spatial dispersion is responsible for the shifting of the upper Davydov component.

ii) *Strongly phase matched SHG* For $\mathbf{k} \| \mathbf{b}$ we have shown, section V, that SHG is not possible. Since the **b**(**a*****a***) and **c**′(**bb**) spectra exhibit very similar vibrational intensity distributions and frequencies our vibronic coupling analysis based on the latter spectrum should not be affected by SHG. However, in our opinion the shifts to higher energy of the center of gravity of the so-called upper component for the $\mathbf{k} \| \mathbf{c}^*$ and $\mathbf{k} \| \mathbf{a}^*$ spectra relative to its position in the $\mathbf{k} \| \mathbf{b}$ spectra, Figures 5, 6, are difficult to reconcile in terms of strongly phase matched SHG. For recall that the vibronic frequencies measured relative to Craig and Gordon's[7] midpoint frequency of 28,627 $cm^{-1}$ are independent of **K** and polarization and, furthermore, that the intensities of Condon fundamentals like 394 and 1020 $cm^{-1}$ relative to the upper component are as well. That is, the upper component behaves like the TPA origin from an intensity point of view. Furthermore, if, for example, the feature at $\sim 120\ cm^{-1}$ in the **c***(**bb**) spectrum, Figure 7, is *not* due to TPA but rather to phase matched SHG one must explain the absence of the upper Davydov component. In view of the vibronic intensities, Table III, for **bb** and the fact that SHG efficiencies would vary markedly with vibronic band such an explanation is not obvious to us. We, therefore, view the possibility of strongly phase matched SHG playing a significant role in the diagonally polarized spectra as slight. Thus, we suggest that what we have for convenience been referring to as the upper Davydov component in Figures 5–8 is primarily a manifestation of TPA. At this point we cannot exclude the possibility that non-phase matched SHG is contributing to the upper component profile but, again, based on the vibronic intensity analysis we believe such a contribution must be small.

iii) *The exciton-phonon interaction* The most important intermediate exciton states in the TPA to the upper Davydov component are expected to be strongly dipole allowed. The exciton bandwidths associated with these states are correspondingly large, several thousand $cm^{-1}$.[18,24,27] Thus, the exciton branch spatial dispersions and $\mathbf{k} = 0$ branch energies will in general have a strong dependence on the sense of **k**. In the TPA experiment one is essentially controlling this sense for the intermediate states through selection of the incident photon wavevector **K**. In the static lattice approximation the selection rule $\mathbf{k} = \mathbf{K} \approx 0$ prevails for pure exciton transitions. With this approximation we saw earlier that for the diagonally polarized TPA spectra the lower

Davydov component is forbidden, consistent with the observed spectra. We suggest, however, that for a consideration of the upper Davydov component region one should formulate the intermediate state problem in terms of composite exciton-phonon states dictated by the exciton-phonon interaction. Because this interaction depends on the details of the phonon and exciton (in particular) spatial dispersions one can reasonably assert that the contributing intermediate exciton-phonon states depends on the choice for **K**. This being the case then the final exciton-phonon states contributing to the upper Davydov component region are also influenced by this selection. Thus, the upper Davydov component region would depend on **K**. Adding to this is the polarization vector of the incident photons which also determines the nature of the intermediate states reached. The suggestion that there should be an exciton-phonon interaction associated with the upper but not the lower Davydov component is supported by the reflection spectra ($\mathbf{K} \perp \mathbf{ab}$) of Syassen and Philpott.[9] In section V, we calculated $n(\omega)$ for the upper component assuming it to be a single oscillator so as to be able to discuss, in a qualitative way, strongly phase matched SHG. However, Syassen and Philpott find that four oscillators are required to fit the reflectance profile for the upper component. Their frequencies relative to the lower component are 46, 62, 72 and 103 $\mathrm{cm}^{-1}$[9] with the 46 $\mathrm{cm}^{-1}$ oscillator the most intense. Although they do not discuss the nature of these oscillators they assign the one at 46 $\mathrm{cm}^{-1}$ as the upper (zero-phonon) Davydov component. Our feeling is that three of these oscillators must represent composite exciton-phonon transitions. On the other hand the reflectance profile for the lower component can be readily fit using a *single* oscillator model. With regard to the assertion that the polarization vector determines the nature of the exciton-phonon intermediate states reached, the paper by Port *et al.*[28] is supportive. In the one-photon absorption spectra of the lowest triplet exciton of anthracene ($\mathbf{K} \| \mathbf{ab}$), the phonon structures associated with the Davydov components are markedly polarization dependent.[28] These structures are adequately understood in terms of one-particle exciton-phonon transitions dictated by the selection rule $\mathbf{k} + \mathbf{q} = \mathbf{K} \approx 0$, where $\mathbf{q}$ is the phonon wavevector.

A quantitative formulation of the problem (not given here) would begin with the TPA matrix element

$$\sum_{I} \sum_{\mu,\mathbf{k}} \sum_{\mathbf{q}_1,\mathbf{q}_2,} \sum_{n_1^i,n_2^i} \boldsymbol{\varepsilon}_2 \cdot \langle F_{\mu'}(\mathbf{k}'); n_1^f(\mathbf{q}_1') \ldots n_j^f(\mathbf{q}_j') \ldots | \mathbf{J}_\perp(\mathbf{K}_2) |$$
$$I\mu(\mathbf{k}); n_1^i(\mathbf{q}_1) \ldots n_j^i(\mathbf{q}_j) \ldots \rangle \langle I\mu(\mathbf{k}); n_1^i(\mathbf{q}_1) \ldots | \mathbf{J}_\perp(\mathbf{K}_1) | G; n_1^g(\mathbf{q}_1'') \ldots \rangle \cdot \boldsymbol{\varepsilon}_1$$
$$\times \left[ E_{I\mu(\mathbf{k}),n_1^i(\mathbf{q}_1)} \ldots - E_1 \right]^{-1} + d_{1 \leftrightarrow 2}. \tag{13}$$

$F$, $I$ and $G$ label the final, intermediate and ground electronic states with $\mu$ and $\mathbf{k}$ the exciton branch and wavevector, respectively. $n_j^f(\mathbf{q}_j')$, for example,

is the number of quanta of the phonon mode associated with the $j$th branch and wavevector $\mathbf{q}'_j$ and the final ($f$) state. The transition operator $\mathbf{J} \perp (\mathbf{K})$ has the form[18]

$$\mathbf{J}_\perp(\mathbf{K}) = \sum_{l\beta} \mathbf{d}^\perp_{l\beta} e^{i\mathbf{k}\cdot\mathbf{l}} \tag{14}$$

in the electric dipole approximation. $\mathbf{l}$ and $\beta$ label the unit cell and unit cell site, respectively, while $\mathbf{K}$ is the photon wavevector. $\mathbf{d}^\perp_{l\beta}$ is the component of the electric dipole moment operator for molecule $l\beta$ transverse to the photon propagation direction.

Equation (13) represents the matrix element for a transition from a specific initial state to a specific final state so to obtain the TPA profile one would sum over all initial phonon levels and final exciton-phonon states for the upper exciton branch, then square and thermally average. If the exciton-phonon states are of the one-particle type (correlated exciton and phonon motion) then the pseudomomentum selection rule is that the sum of the exciton and phonon wavevectors must be conserved during each one-photon process.[28] Thus, one can in principle reach the entire $\mathbf{k}$ spectrum of the intermediate exciton branches through creation of phonons. This holds also for the final exciton-phonon states. The associated probabilities depend on the details of the exciton-phonon interaction which depends on $\mathbf{K}$ and the photon polarization. We suggest, therefore, that the exciton-phonon interaction is mainly responsible for the $\mathbf{K}$ and polarization dependence of the upper Davydov component region. Individual peaks, when observed, are most likely due to one-particle exciton-phonon transitions. Apparently, the variation of the strength of the exciton-phonon interaction with $\mathbf{K}$ and polarization would be responsible for the motion of the center of gravity for the upper component. We hope to be able to present a more quantitative discussion of this problem and others associated with the TPE spectra of phenanthrene's 350 nm state in the near future.

## Acknowledgments

The support of the Quantum Chemistry Division of NSF and Basic Energy Sciences of the U.S.D.O.E. for this work is gratefully acknowledged. So too is the experimental assistance of E. S. Yeung and O. Kallman during the early stages of the project.

## References

1. R. M. Hochstrasser and G. R. Meredith, *J. Chem. Phys.*, **67**, 1273 (1977).
2. R. M. Hochstrasser and G. R. Meredith, *J. Lumin*, **18/19**, 32 (1979).
3. R. M. Hochstrasser, C. M. Klimcak, and G. R. Meredith, *J. Chem. Phys.*, **70**, 870 (1979).
4. A. Bree, M. Edelson, and C. Taliani, *Chem. Phys.*, **30**, 343 (1978).
5. V. L. Broude, E. I. Rashba, and E. F. Sheka, *Phys. Status Solidi*, **19**, 395 (1967), and earlier references described therein.

6. V. L. Broude, W. S. Medvedev, and A. F. Prokhot'ko, *Zh. Eksp. Theor. Fiz.*, **21**, 665 (1951).
7. D. P. Craig and R. D. Gordon, *Proc. Roy. Soc. London Ser.*, **A288**, 69 (1965).
7. R. M. Hochstrasser and G. J. Small, *J. Chem. Phys.*, **45**, 2270 (1966).
9. K. Syassen and M. R. Philpott, *J. Chem. Phys.*, **69**, 1251 (1978).
10. D. P. Craig and G. J. Small, *J. Chem. Phys.*, **50**, 3827 (1969).
11. H. Mahr, in *Quantum Electronics Vol. I*, ed. by H. Rabin and C. L. Tang, (Academic, New York 1975), Chapter 4.
12. R. Mason, *Mol. Phys.*, **4**, 413 (1961).
13. R. M. Hochstrasser and H. N. Sung, *J. Chem. Phys.*, **66**, 3276 (1977).
14. B. J. McArdle, J. N. Sherwood, and A. C. Damask, *J. Cryst. Growth*, **22**, 193 (1974).
15. A. N. Winchell, *Optical Properties of Organic Compounds*, (Academic, New York, 1954).
16. V. SethuRaman, G. J. Small, and E. S. Yeung, *Rev. Sci. Instrum.*, **48**, 106 (1977).
17. H. Otokozawa, S. Inomata, N. Mikami, and M. Ito, *Bull. Chem. Soc. Jpn.*, **50**, 2899 (1977).
18. A. S. Davydov, *Theory of Molecular Excitons*, (Plenum, New York, 1971).
19. Prof. K. Ruedenberg, Dept. of Chemistry, Iowa State University, Ames, Iowa 50011, private communication.
20. Details available upon request.
21. C. A. Coulson and A. Streitwieser, Jr., *Dictionary of π-electron Calculations*, (Freeman, San Francisco 1965).
22. e.g. $D = 1.00$ and *no* frequency change between the ground and excited state corresponds to a FC factor of 0.5 for the $0 \rightarrow 1$ transition.
23. G. J. Small, *J. Chem. Phys.*, **62**, 4661 (1975).
24. D. P. Craig and S. H. Walmsley, *Excitons in Molecular Crystals*, (Benjamin, New York, 1968).
25. M. R. Philpott, *J. Chem. Phys.*, **50**, 5117 (1969).
26. M. R. Philpott and J. W. Lee, *J. Chem. Phys.*, **58**, 595 (1973).
27. M. R. Philpott, *J. Chem. Phys.*, **54**, 111 (1971).
28. H. Port, D. Rund, G. Small, and V. Yakhot, "The Exciton-Phonon Interaction for Triplet Exciton Bands of Organic Solids: An Experimental and Theoretical Study", *Chem. Phys.*, in press.